Polymer Testing 114 (2022) 107711

Contents lists available at ScienceDirect

Polymer Testing

journal homepage: www.elsevier.com/locate/polytest

Composite materials with MWCNT processed by Selective Laser Sintering for electrostatic discharge applications

A.C. Lopes [a,b,*], A.M. Sampaio [a,b,c], A.J. Pontes [a,b]

[a] IPC – Institute for Polymers and Composites, University of Minho, Guimarães, Portugal
[b] DONE Lab – Advanced Manufacturing of Products and Tools, University of Minho, Guimarães, Portugal
[c] Lab2PT, School of Architecture, University of Minho, Guimarães, Portugal

ARTICLE INFO

Keywords:
Additive manufacturing
Selective laser sintering
Composite materials
Polyamide 12
MWCNT
Electrostatic discharge

ABSTRACT

Selective Laser Sintering (SLS) is an additive manufacturing technology that enables the production of polymeric parts for end-use applications. Despite the great potential of conventional materials, carbon-based reinforcements have been widely considered to contradict the electrically insulating nature of polymers, allowing the applicability of SLS in novel applications within electronics industry. However, the laser-sintering processing of such materials still encompasses a number of limitations including agglomeration problems, weak interparticle adhesion, low parts resolution, high processing time and costs. Therefore, this research reports the development of functional composite materials for SLS capable of being considered for the production of components that are in direct contact with electrostatic discharge (ESD) sensitive devices. To do so, composite materials of Polyamide 12 incorporating 0.50 wt%, 1.75 wt% and 3.00 wt% of Multi-Walled Carbon Nanotubes were developed aiming to achieve values of surface resistance between 10^4 - 10^9 Ω, according to the delivery instructions of Bosch Car Multimedia S.A. Test specimens produced by SLS were dimensionally, mechanically, electrically, thermally and morphologically characterized. Comparing to the neat matrix, the composite materials revealed narrower SLS processing window, reduced mechanical strength, surface resistance in the ESD range and electrical conductivity until 10^{-6} S/cm. Fundamentals on the sintering process of these functional materials are also provided.

1. Introduction

Selective Laser Sintering (SLS) makes use of powder material sintered by the thermal energy of a laser source to additively produce polymeric parts [1]. Since this powder bed fusion process involves complex thermal mechanisms, SLS materials need to comply with a series of requirements to be successfully processed [2,3]. For laser-sintering, preference should be given to semi-crystalline thermoplastics with a distribution of particles size between 45 and 90 μm, a large range between the melting and crystallization temperatures (*i.e.* processing window), great heat resistance, low melting viscosity and low surface tension [2,4–7]. Due to their ability to meet most of these requirements and valuable processability-property-cost compromise, polyamides are materials of first choice [2,8]. Despite the great performance of the conventional solutions, composite materials with enhanced properties and new functionalities are continuously being required for novel applications [8–10]. Comparing with other additive manufacturing technologies, SLS has advantageous characteristics to include these alternative materials. As the process does not involve compacting sources or shear forces, the aspect ratio of reinforcements is not significantly modified during the sintering allowing to achieve promising results with low percolation thresholds [11,12]. Most of the properties of composite materials with significant impact on the laser-sintering process (*e.g.* morphology, flowability, surface energy) are dependent on three main interrelated factors: *i*) properties of all constituents, *ii*) matrix-reinforcement ratio and *iii*) preparation and processing methods [2,13,14]. There is a wide selection of methods to prepare materials for SLS based on different principles of operation and degree of complexity, such as spray drying, precipitation of solutions, milling-based methods at cryogenic temperatures, melt-compounding combined with milling procedures and mechanical mixing [8,14]. Mechanical mixing is one of the most common method since it is attractive for simple, quick and economic preparations; however, efficient and uniform mixtures can be challenging to obtain when powders with different sizes and densities need to be combined [2,8]. Depending on the composite materials, these methods can also be complemented with

* Corresponding author. IPC – Institute for Polymers and Composites, University of Minho, Guimarães, Portugal.
E-mail address: acarinalopes@dep.uminho.pt (A.C. Lopes).

https://doi.org/10.1016/j.polymertesting.2022.107711
Received 9 May 2022; Received in revised form 7 June 2022; Accepted 16 July 2022
Available online 21 July 2022

Table 1
Process parameters selected for the experiments.

HATCHING	Laser power (W)	32
	Scan speed (mm/s)	3730
	Hatch distance (mm)	0.30
	Extra beam offset (mm)	0.12
CONTOUR AND POST CONTOUR	Scan speed (mm/s)	3000
	Laser power (W)	34
	Extra beam offset (mm)	0
EDGES AND POST EDGES	Edge factor	1.80
	Scan speed (mm/s)	1500
	Laser power (W)	20
Layer thickness (mm)		0.12
Process chamber temperature (°C)		173
Removal chamber temperature (°C)		130
Beam offset (mm)		0.32
Material dependent scaling (%)	X	3.25
	Y	3.18
	Z (0)	2.55
	Z (600)	1.40

pre-treatments or pre-modifications of the reinforcement to maximize the adhesion with the matrix, using chemical and/or thermal approaches [15–17]. Concerning the constituents and because of polymers are insulating materials, carbon-based composites are one of the most explored to be used in SLS [15,18,19]. In fact, conductive polymeric materials are being considered modern alternative solutions to conventional metals for advanced applications, such as lightweight and corrosion resistant shielding structures aiming the protection of electronic equipment in automotive or medical fields [20]. Focusing on their potential for such applications, various solutions integrating carbon nanotubes, carbon fibres, carbon black, graphite or graphene have been extensively reported in literature due to their ability to establish strong interactions with polymeric matrices and homogenous distributions and dispersions, resulting in composite parts with superior mechanical, thermal and electrical properties [15]. Carbon-based composites combining Polyamide 12 (PA12) with Multi-Walled Carbon Nanotubes (MWCNT) has expanded in the last few years. Salmoria *et al.* [21] used mechanical mixing for 70 min to develop composite materials of PA12 with 0.5 wt% of MWCNT. As a result, parts produced with this material exhibited 10% higher flexural tensile strength and 11-9% lower flexural elongation than parts produced with neat-PA12. Later, Salmoria *et al.* [19] evaluated the incorporation of 0.5 wt%, 1.0 wt% and 3.0 wt% of MWCNT in the PA12 matrix using similar preparation methods. In their experiments, parts produced with 1.0 wt% of MWCNT showed flexural strength 25.8% higher than neat-PA12 parts. The mechanical strength decreased with the incorporation of 3.0 wt% of MWCNT while the electrical resistivity significantly decreased until 5.4×10^6 Ω cm. Bai *et al.* [22] used a specific coating method to prepare PA12-MWCNT composites. In initial studies, composite parts of PA12 with 0.1 wt% of MWCNT presenting elastic modulus and density respectively 54% and 4.1% higher than neat-PA12 parts were developed. After that, Bai *et al.* [23] extended the analysis to composite materials containing 0.2 wt% of MWCNT. The results revealed values of melting viscosity between 300 and 900 Pa·s depending on the temperature and 20% higher dynamic elastic modulus. In a following research, Bai *et al.* [24] evaluated the thermal properties of PA12 incorporating 0.1 wt% of MWCNT. An increase of 14.2% in the thermal conductivity until 0.13 $WK^{-1}m^{-1}$ (depending on the temperature) was obtained, comparing to neat-PA12 parts. Paggi *et al.* [25] developed PA12 materials with 0.5 wt%, 1.0 wt% and 3.0 wt% of MWCNT through magnetic stirring of solutions and mechanical mixing. The findings obtained through ANOVA analyses revealed that an optimized incorporation of 1.7 wt% of MWCNT combined with adjusted process parameters is suitable to produce quality composite parts by SLS. Through precipitation of solutions, Yuan *et al.* [26] developed PA12 with 0.5 wt% of MWCNT that were pre-modified with sodium cholate. As outputs, the authors obtained composite parts with tensile strength, elastic modulus and toughness respectively 31.8%, 0.8% and 84.9% higher than neat-PA12 parts. In another research, Yuan *et al.* [27] used the same pre-treatments and preparation methods to develop composites of PA12 incorporating 0.1 wt%, 0.5 wt% and 1.0 wt % of MWCNT. Composite parts with 0.5 wt% of MWCNT revealed the greatest outcomes, showing 10^{-5} S/cm of electrical conductivity and 0.40 $WK^{-1}m^{-1}$ of thermal conductivity. In general, research conducted in this field revealed that the inclusion of MWCNT significantly influences the melting viscosity, flowability, sintering window, efficiency to absorb the energy of the laser beam and, consequently, properties of the polymeric base material in which they are incorporated [21,23,26]. However, despite the promising results that have been reported in the last years, there are still some limitations regarding this class of materials, such as *i*) complex processing, *ii*) agglomeration and non-uniform distribution and dispersion of reinforcements, *iii*) weak interparticle adhesion *iv*) low parts resolution, *v*) high costs and *vii*) long processing time [13,16]. In this way, the purpose of this research is to explore composite materials produced with PA12 incorporating MWCNT in the weight percentages of 0.50 wt%, 1.75 wt% and 3.00 wt%. Initial studies focused on establishing suitable conditions of preparation and processing, contradicting common limitations. In order to be cost-effective, the composite materials were prepared through mechanical mixing in a continuous and systematic method and further processed in a laser-sintering equipment with adjusted values of energy density. Experiments with neat-PA12 material were carried out for reference. The dimensional, mechanical, thermal, electrical and morphological properties of test specimens produced with the developed materials were evaluated to in detail identify the influence of the incorporation of MWCNT on the polymeric matrix. Based on the employed methodology, a comprehensive understanding regarding the challenges and opportunities in processing these functional materials by SLS is provided. Focusing on the current needs of the electronics industry, the potential of these solutions for non-conventional applications where protection against electrostatic discharges (ESD) is required was also explored, based on the internal Bosch Car Multimedia S.A. norm. The technical instructions of the company refer to values of surface resistance between 10^4 and 10^9 Ω for components in direct contact with ESD sensitive devices. The novelty in the development of composite materials for application at industrial reality contradicts most of the research in the

Fig. 1. Details of the top surface of test specimens produced by SLS with PA12 incorporating 0.50 wt% (left), 1.75 wt% (top) and 3.00 wt% (right) of MWCNT.

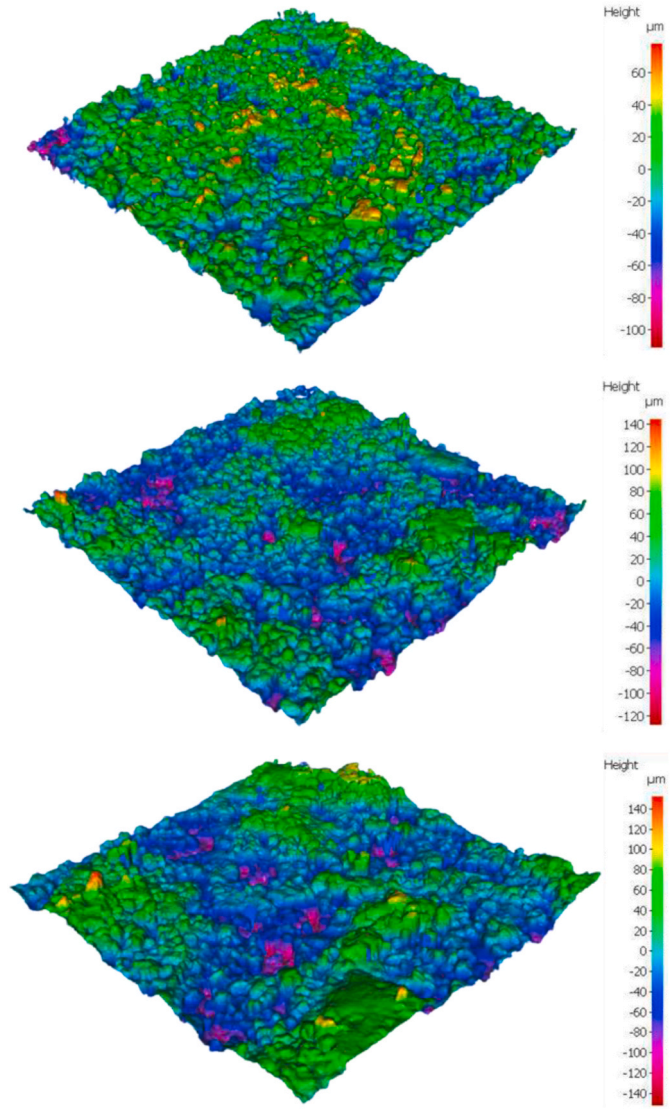

Fig. 2. Top surface topography of test specimens produced by SLS with PA12 incorporating 0.50 wt% (top), 1.75 wt% (middle) and 3.00 wt% (bottom) of MWCNT.

field which is currently limited to laboratory investigation for scientific purposes [28]. This provides a valuable knowledge base for the implementation of additive manufacturing components suited to advanced requirements demanded by industrials with promising benefits in terms of productivity, flexibility and costs.

2. Materials and methods

2.1. Materials

PA12 powder (*i.e.* PA 2200 from EOS GmbH) with average particle size of 56 µm, bulk density of 0.45 g/cm^3 and laser-sintered density of 0.93 g/cm^3 in a mixture ratio of 50:50% was used as polymeric matrix [29]. MWCNT (*i.e.* NC7000™ from NANOCYL) with nominal average dimensions of 9.5 nm of diameter and 1.5 µm of length was used as carbon-based reinforcement [30]. The weight percentages of 0.50 wt%, 1.75 wt% and 3.00 wt% of MWCNT were considered, seeking for the minimum amount of reinforcement capable to reduce the electrical resistance and resistivity of the matrix, without compromising its thermal and mechanical properties. Experiments with neat-PA12 material were considered as reference condition.

2.2. Preparation and processing

In order to avoid high development costs, the composite materials were prepared through mechanical mixing in a continuous process at 15 rpm for 12 h at 23 °C in a 3devo AIRID operating with a self-sufficient mixing system by means of a stirring rotator. After preparation, the composite materials were processed in an EOS P 396 laser-sintering machine equipped with a vibrating powder dispenser with adjusted fluidisation flow rate (*i.e.* 15 l/min) to minimize compaction effects. Table 1 summarizes the process parameters that were selected to process the composite materials, defining a medium-low energy value of 0.238 J/mm^3, as well as the material dependent scaling adjusted to the PA12 matrix. These values were prior optimized for the conditions of the study.

The test specimens required for characterization were positioned in the XYZ orientation in the centre of the building platform to ensure maximum thermal stability. Once produced and cooled, the test specimens were cleaned with compressed air in a blasting station and stainless-steel magnetic polishing pins in a polishing station. Until testing, the test specimens were stored in a controlled environment of 22 °C and 40 rH%.

2.3. Characterization tests

2.3.1. Surface roughness characterization

The average surface roughness of the test specimens produced with the composite materials was determined through optical 3D measurements based on the Focus-Variation technology using an InfiniteFocusSL Alicona microscope operating with a 10x objective magnification with lateral topographic resolution of 2 µm.

2.3.2. Dimensional characterization

The mass of five test specimens per condition was measured in a KERN Precision balance and their thickness, width and length were determined through an average of three different points using a GARANT DC2 calliper.

2.3.3. Mechanical characterization

The mechanical properties were evaluated in five test specimens per condition through tensile, compression and v-notch Izod impact tests. An Instron 5969 Universal Testing System operating with a load cell of 50 kN at room temperature was used to conduct the tensile tests at 1 mm/min (test specimens 1BA (ISO 527–2)) and compression tests at 1.3 mm/min (test specimens modelled according to ASTM D695) [31,32]. Corrections for slack, alignment and seating effects were applied on the resulting stress-strain curves. The v-notch Izod impact tests (Test Method A, ASTM D256) were performed in a CEAST Impact Testing

Table 2
Surface roughness parameters of PA12-MWCNT composites processed by SLS.

	Arithmetic mean height, Sa (µm)	Maximum peak height, Sp (µm)	Maximum valley depth, Sv (µm)
PA12 + 0.50 wt% MWCNT	13.5	65.4	71.7
PA12 + 1.75 wt% MWCNT	15.5	110.2	96.6
PA12 + 3.00 wt% MWCNT	16.1	117.1	107.7

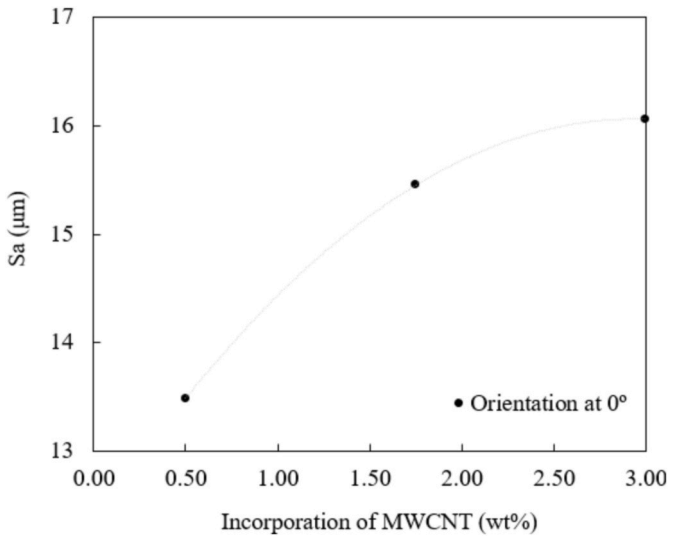

Fig. 3. Arithmetic mean height (Sa) of the top surface of test specimens produced by SLS as a function of the incorporation of MWCNT.

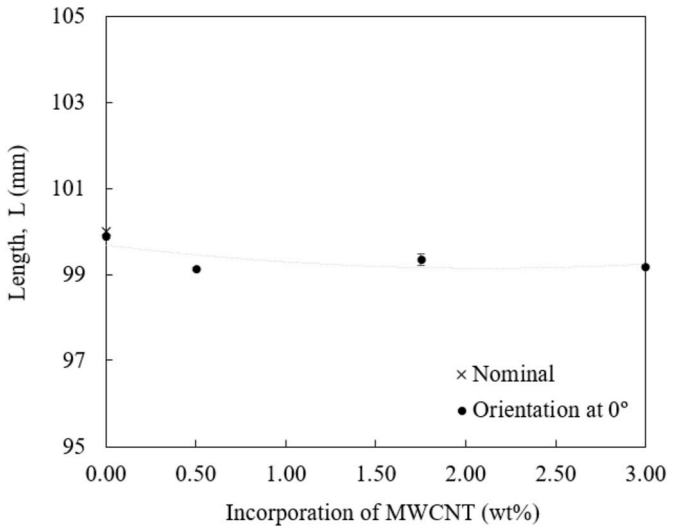

Fig. 4. Length of test specimens produced by SLS as a function of the incorporation of MWCNT.

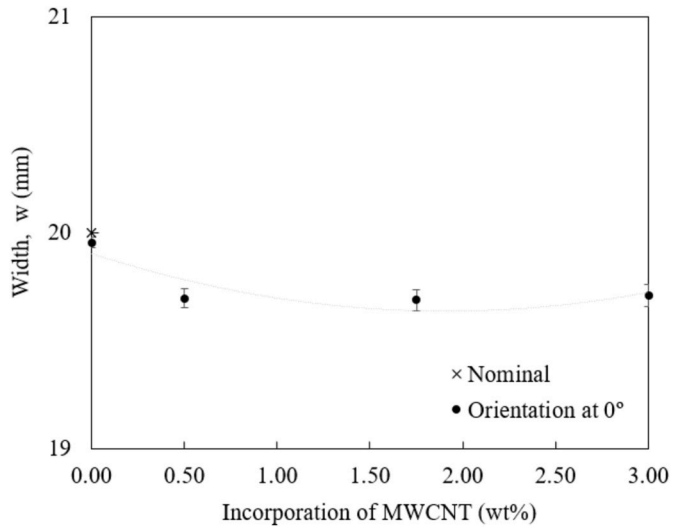

Fig. 5. Width of test specimens produced by SLS as a function of the incorporation of MWCNT.

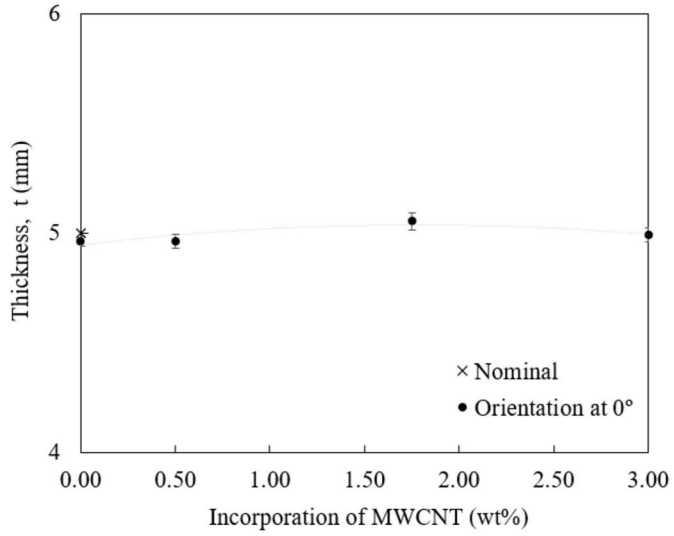

Fig. 6. Thickness of test specimens produced by SLS as a function of the incorporation of MWCNT.

Machine at room temperature using a pendulum with 4 J of capacity [33]. Windage and friction effects were excluded.

2.3.4. Electrical characterization

The electrical resistance and resistivity of the developed materials were determined in a Keithley Model 8009 Resistivity Test Fixture operating at 10 V through an average of 100 readings in test specimens with nominal dimensions of 100 × 100 × 1.5 mm (designed according to the electrode configuration) through surface and volume measurements. The measurements were based on the standard test norm ASTM D257.

2.3.5. Thermal characterization

To identify the thermal processing window of the composite powder materials, their melting and crystallization temperatures were assessed through Differential Scanning Calorimetry (DSC). The analyses were carried out in a Netzsch DSC 200 F3 Maia using 2 - 40 mg of sample (ISO 11357 [34]) according to the following scanning program: *i*) isothermal of 1 min at 30 °C, *ii*) first heating at 10 °C/min from 30 °C to 230 °C, *iii*) isothermal of 1 min at 230 °C, *iv*) cooling at 10 °C/min from 230 °C to 30 °C, *v*) isothermal of 1 min at 30 °C and *vi*) second heating at 10 °C/min to 230 °C, under a nitrogen atmosphere. Furthermore, a TA Q500 was used to perform a Thermogravimetric Analysis (TGA) in order to evaluate the thermal stability of the composite materials during a heating program at 10 °C/min, from 40 °C to 700 °C, under a nitrogen atmosphere, according to the standard test method ASTM E1131 [35].

2.3.6. Morphological characterization

Scanning Electron Microscopy (SEM) analyses were performed to evaluate the dispersion and distribution of the carbon-based reinforcements in the polymeric matrix and resulting content of porosity of the cross-section. The measurements were taken in a Nano SEM FEI Nova 200 equipment operating with an acceleration voltage of 10 kV. Before the analysis, the samples were prepared with 15 nm of gold coating.

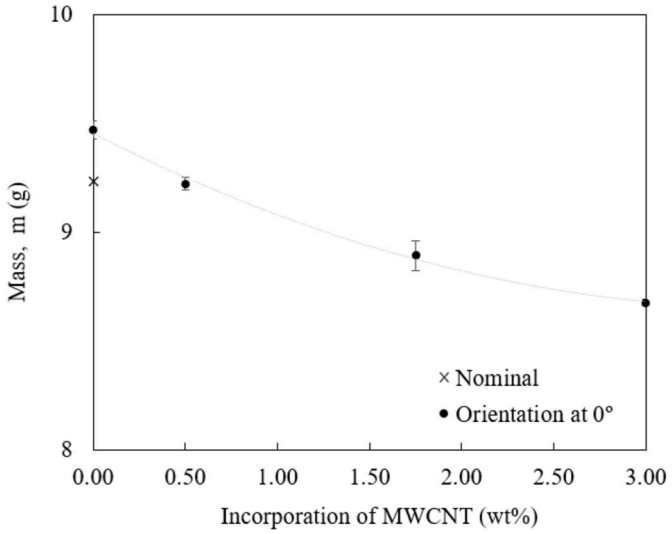

Fig. 7. Mass of test specimens produced by SLS as a function of the incorporation of MWCNT.

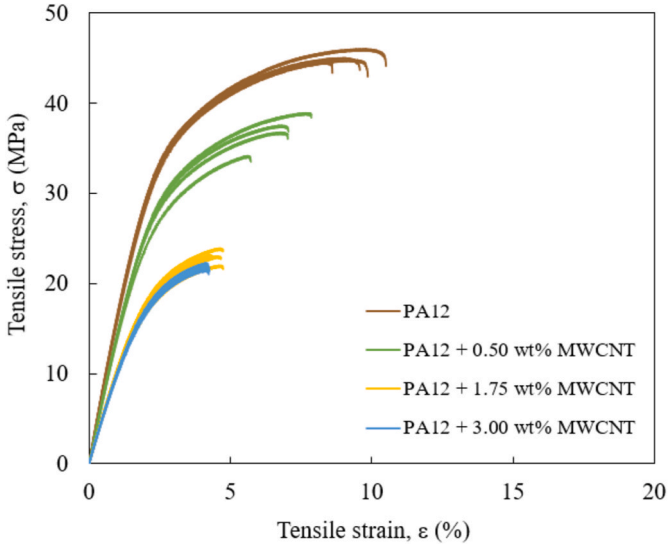

Fig. 8. Engineering stress-strain curves of test specimens produced by SLS as a function of the incorporation of MWCNT.

3. Results and discussion

3.1. Description of observations

The experiments carried out to assess the performance of PA12-MWCNT composites provided useful insights in relation to their preparation and processing. The initial stage of materials preparation demonstrated that as the amount of MWCNT increases, homogeneous powder mixtures become more difficult to obtain, considering same periods of mixing. This was verified through the higher amount of unmixed reinforcement migrated to the top and outer edges of the powder mixture in the mixing hopper. In order to minimize this effect, the automatic procedure was complemented with manual mixing. With regard to the laser-sintering, the experiments demonstrated that the complexity of processing increases with the increasing of powder compaction effects, since the powder has to flow from upper feed containers to the building platform. Laser-sintering machines where the powder is spread from lower feed containers that rise to a height corresponding to the layer thickness could simplify the sintering of these

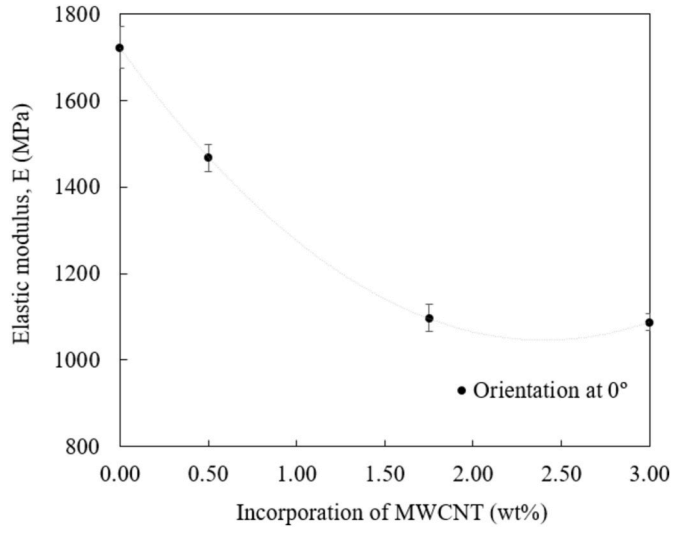

Fig. 9. Elastic modulus of test specimens produced by SLS as a function of the incorporation of MWCNT.

composite materials. In terms of process parameters, it was verified that the value of energy density needed for a successful sintering process gradually decreases as the amount of MWCNT increases. High values of energy supplied to polymeric materials integrating a large amount of carbon-based reinforcement intensifies the thermal gradients inside the building chamber. This agrees with results obtained by Salmoria *et al.* [21] and Bai *et al.* [22,24]. In this work, 0.238 J/mm^3 was found as the maximum allowable value to process PA12 material incorporating 0.50 wt%, 1.75 wt% and 3.00 wt% of MWCNT. Once optimized, the sintering process proceeded normally. The initial observations evidenced differences in colour between test specimens which become darker with the increasing amount of MWCNT. Different surface finishing was also observed between the test specimens produced (Fig. 1). With greater amounts of MWCNT, the tactile perception suggested an increase of roughness due to the higher number of carbon-based particles migrated to the external surfaces of the test specimens, which also resulted in more difficult cleaning steps after the sintering process.

3.2. Surface roughness characterization

Fig. 2 shows the topography of the top surface of test specimens produced by SLS with the developed composite materials. In a first observation, it is possible to detect an increase in the range of height between peaks and valleys in relation to the midplane of the test specimens with the incorporation of MWCNT (denoted by the colouring gradient), which directly influences the surface roughness parameters (Table 2). For an elected area of the upward-facing surface, the test specimens produced with PA12 incorporating 0.50 wt%, 1.75 wt% and 3.00 wt% of MWCNT respectively presented values of arithmetic mean height (Sa) of 13.5 μm, 15.5 μm and 16.1 μm in a rising trend (Fig. 3). Optical measurements of the surface roughness of a similar PA12 material showed Sa values between 14 and 18 μm [36]. This demonstrates that the test specimens produced with the PA12-MWCNT composite materials developed in this work exhibited values of surface roughness in the order of magnitude expected for laser-sintered parts but with tendency to increase with the increasing weight percentage of MWCNT until 20% from 0.50 wt% to 3.00 wt%.

3.3. Dimensional characterization

The results of dimensional characterization showed that the incorporation of MWCNT did not induce significant modifications in the length (Fig. 4), width (Fig. 5) and thickness (Fig. 6) of parts produced by

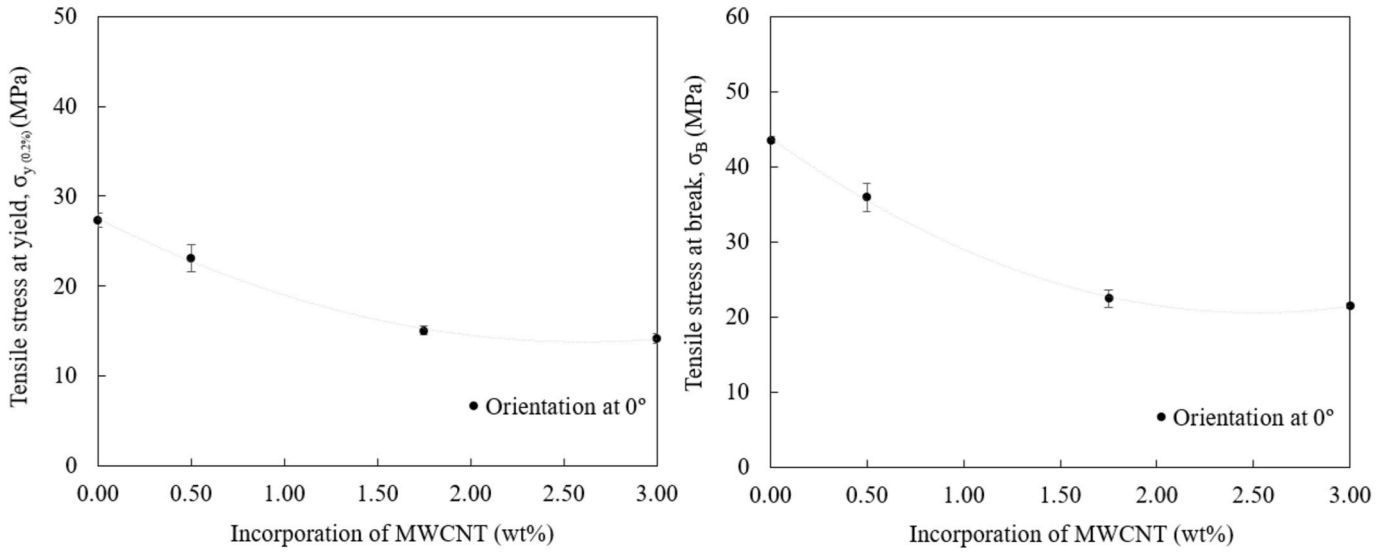

Fig. 10. Tensile stress at yield (left) and break (right) of test specimens produced by SLS as a function of the incorporation of MWCNT.

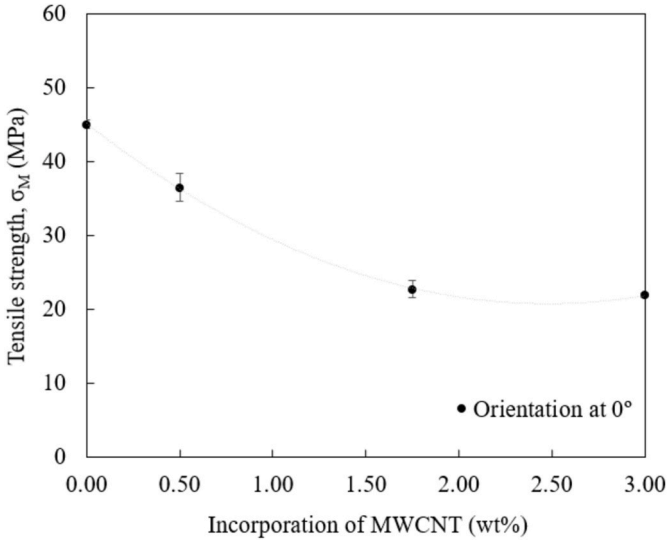

Fig. 11. Tensile strength of test specimens produced by SLS as a function of the incorporation of MWCNT.

SLS. In the experiments conducted in this research, test specimens produced with composite materials presented great dimensional accuracy, with dimensions similar to the nominal 100 mm in length, 20 mm in width and 5 mm in thickness. Slight variations could be a result of the differences in the thermal gradients of processing, comparing to the conventional material. In turn, the mass of test specimens produced with composite materials gradually decreased with the increasing amount of MWCNT from 0.50 wt% to 3.00 wt% (Fig. 7). The highest variation was observed in test specimens produced with 3.00 wt% of MWCNT that recorded a mass of 8.675 ± 0.015 g, significantly inferior to the mass of test specimens produced with neat-PA12 (*i.e.* 9.470 ± 0.040 g). This maximum difference of 8.4% is justified by the low bulk density of MWCNT (*i.e.* 0.070–0.075 g/cm^3 (according to NANOCYL)), in comparison to the bulk density of the neat-PA12 used in this work (*i.e.* 0.45 g/cm^3). This indicates that higher incorporations of MWCNT results in SLS parts with low density, suggesting the potential of such materials for applications were lightweight is the most critical factor.

3.4. Mechanical characterization

The mechanical characterization revealed the significant effect of the MWCNT on the mechanical performance of parts produced by SLS. Fig. 8 shows representative engineering stress-strain curves obtained from tensile tests carried out in test specimens produced with neat-PA12 and PA12 with 0.50 wt%, 1.75 wt% and 3.00 wt% of MWCNT.

The results showed that the tensile properties decrease with the increasing amount of MWCNT incorporated in the polymeric matrix with less pronounced variation between the conditions of 1.75 wt% and 3.00 wt%. Regarding the elastic modulus, the results revealed a maximum decrease of 37% from 1723.6 ± 48.2 MPa in test specimens produced with neat-PA12 to 1088.0 ± 19.6 MPa in test specimens produced with 3.00 wt% of MWCNT (Fig. 9).

The tensile stress at yield, tensile stress at break and tensile strength also decreased with the amount of MWCNT (Figs. 10 and 11). Comparing to neat-PA12 parts, the reduction in these mechanical properties reached 50% until the condition with the highest amount of MWCNT. The maximum decrease was verified from test specimens produced with 0.50 wt% of MWCNT to test specimens produced with 1.75 wt% of MWCNT. Between 1.75 wt% and 3.00 wt% of MWCNT the tensile stress was similar, until a minimum tensile stress at yield of 14.1 ± 0.6 MPa, a tensile stress at break of 21.5 ± 0.4 MPa and a tensile strength of 21.9 ± 0.3 MPa.

The tensile strain at yield of test specimens produced with 3.00 wt% of MWCNT reduced 17.5% comparing to parts produced with neat-PA12 material (Fig. 12 (left)). Between these conditions, this mechanical property recorded a gradual reduction from 1.9 ± 0.1% to 1.5 ± 0.1%. The variation was higher for the tensile strain at break (Fig. 12 (right)). It decreased a maximum of 57% in test specimens produced with composite materials until 4.2 ± 0.1% comparing to parts produced with neat-PA12 material which exhibited a tensile strain at break of 9.6 ± 0.8%.

The compression tests also demonstrated the influence of the MWCNT in the final properties of the composite materials in relation to the neat polymeric matrix. Representative engineering stress-strain curves obtained from compression tests are shown in Fig. 13.

As verified with the tensile tests, the compressive properties also gradually decreased with the incorporation of MWCNT. The elastic modulus showed a maximum decrease of 34%, from 1511.1 ± 22.1 MPa in neat-PA12 test specimens to 1003.0 ± 51.1 in test specimens incorporating 3.00 wt% of MWCNT (Fig. 14 (left)). In turn, the compressive strength reduced 36% under the same conditions, from 56.5 ± 0.3 MPa

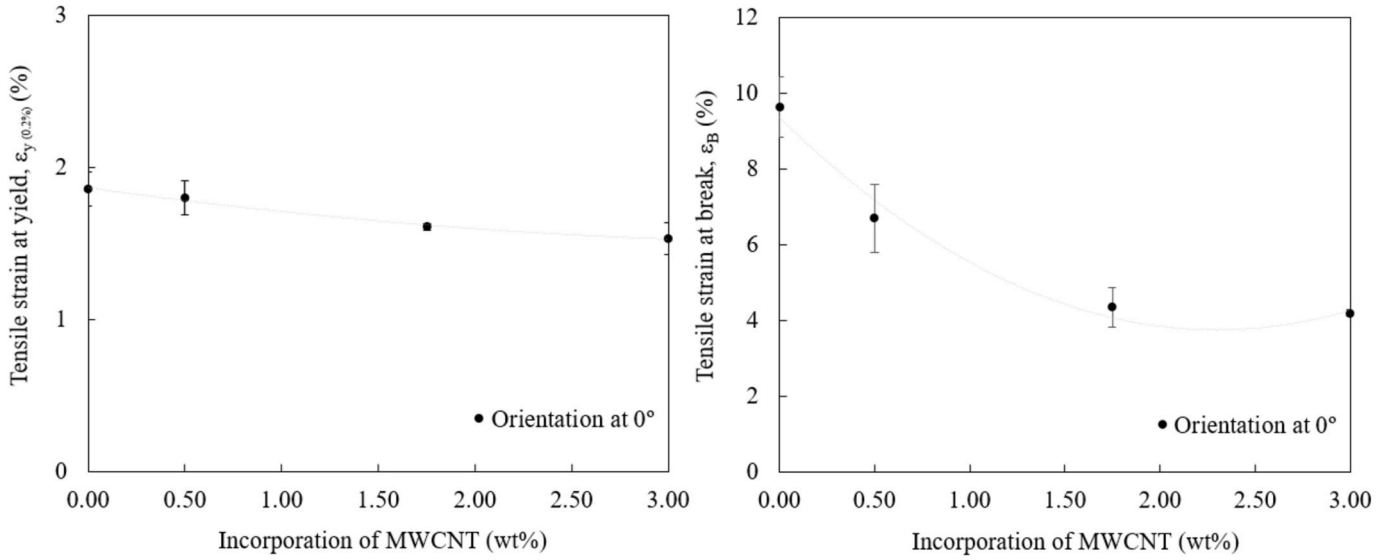

Fig. 12. Tensile strain at yield (left) and break (right) of test specimens produced by SLS as a function of the incorporation of MWCNT.

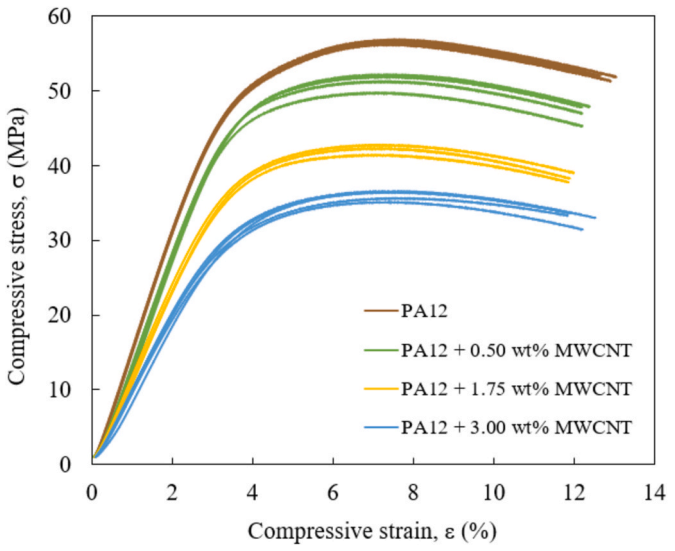

Fig. 13. Engineering stress-strain curves of test specimens produced by SLS as a function of the incorporation of MWCNT.

to 36.0 ± 0.6 MPa (Fig. 14 (right)). The smallest reduction was verified in test specimens produced with 0.50 wt% of MWCNT, which recorded 1299.3 ± 39.5 MPa of elastic modulus and 51.2 ± 1.0 MPa of tensile strength.

In the Izod impact tests, the pendulum with 4 J of capacity promoted the complete break of all test specimens in the section of the v-notch. In this respect, the neat-PA12 parts showed an impact resistance of 5.1 ± 0.3 kJ/m^2, while composite parts reached values between 4.1 and 4.6 kJ/m^2 (Fig. 15). With these results, it is possible to argue that the incorporation of MWCNT does not significantly influences the impact resistance of parts produced by SLS.

3.5. Electrical characterization

The electrical characterization revealed that the surface and volume resistance and resistivity of the test specimens decrease with the amount of MWCNT, while the electrical conductivity gradually increases (Tables 3 and 4, with representation of the standard deviation). The surface resistance of neat-PA12 and PA12 incorporating 0.50 wt% of MWCNT exhibited similar orders of magnitude (*i.e.* 10^{10} Ω), in the insulative range. On the other hand, a significant reduction in the resistivity was verified with the addition of 1.75 wt% and 3.00 wt% of MWCNT to the matrix, reaching values of surface resistance of 10^4 Ω and 10^3 Ω, respectively. In addition, the electrical conductivity increased several orders of magnitude from 10^{-12} S/cm in neat-PA12 parts to 10^{-7} S/cm and 10^{-6} S/cm in parts produced with 1.75 wt% and 3.0 wt% of MWCNT, respectively. The test specimens produced with 1.75 wt% of MWCNT reached the electrostatic dissipative range (*i.e.* 10^4 < surface resistance < 10^9 Ω, according to the internal Bosch Car Multimedia S.A. norm), evidencing the creation of an effective conductive path between the particles of reinforcement allowing to enhance the electrical conductivity of the materials. In turn, test specimens produced with PA12 incorporating 3.00 wt% of MWCNT attained the electrostatic conductive range.

The electrical results obtained from volume measurements are in agreement with the surface measurements. This suggests that the MWCNT are also creating a conductive path for electrical conductivity along the cross-section of the test specimens in order to achieve values of electrical conductivity close to 10^{-7} S/cm and 10^{-6} S/cm using composite materials incorporating 1.75 wt% and 3.00 wt% of MWCNT, respectively.

3.6. Thermal characterization

The melting and crystallization temperatures (*i.e.* T_m and T_c, respectively) of the PA12-MWCNT composite materials determined through DSC are shown in Fig. 16. The DSC measurements revealed that T_m is not significantly affected by the incorporation of MWCNT, recording values close to 177 °C for all composite materials. In turn, T_c increased from 145 °C in neat-PA12 to 151.1 ± 0.2 °C in MWCNT-based composite materials. This difference reduced the interval between T_m and T_c, and, consequently, the SLS processing window in 6 °C. This means that while the conventional PA12 material can be processed within an interval of 32 °C, the composite materials developed in this research may only be processed in a range of 26 °C. In this work, this result did not affect the sintering as the processing temperature was fixed in 173 °C in all building jobs.

The onset temperature obtained by TGA analysis did not reveal substantial differences in the thermal stability of the developed materials (Fig. 17 (left)). This characteristic deflection point reached values close to 400 °C in all TGA thermograms. Bellow that temperature, the

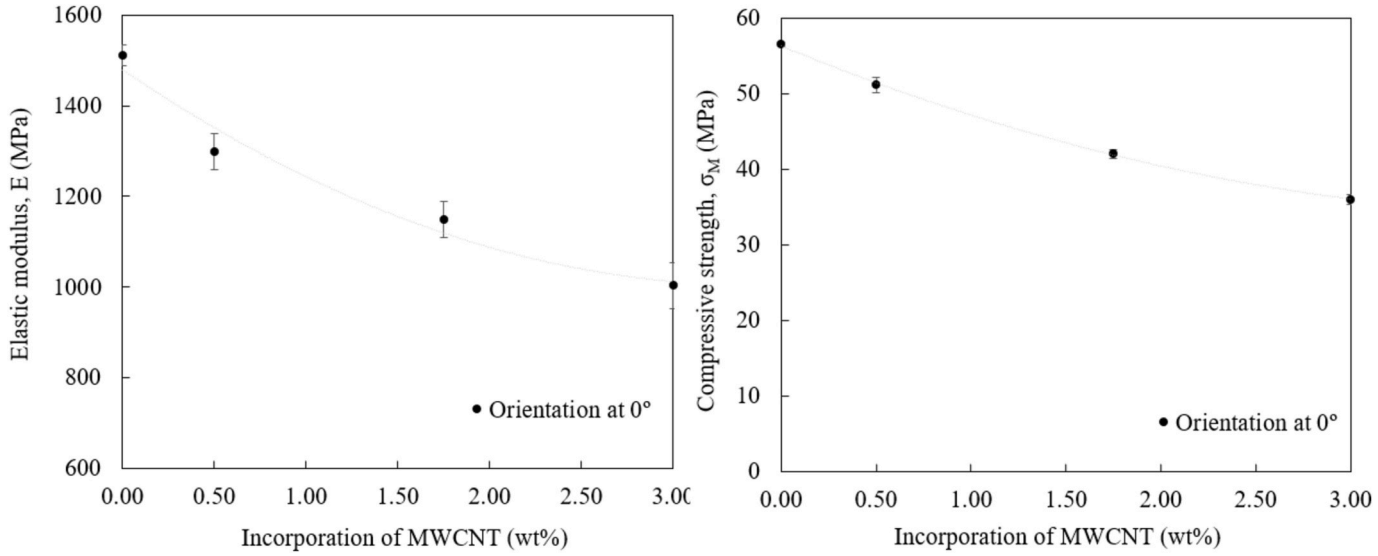

Fig. 14. Elastic modulus (left) and compressive strength (right) of test specimens produced by SLS as a function of the incorporation of MWCNT.

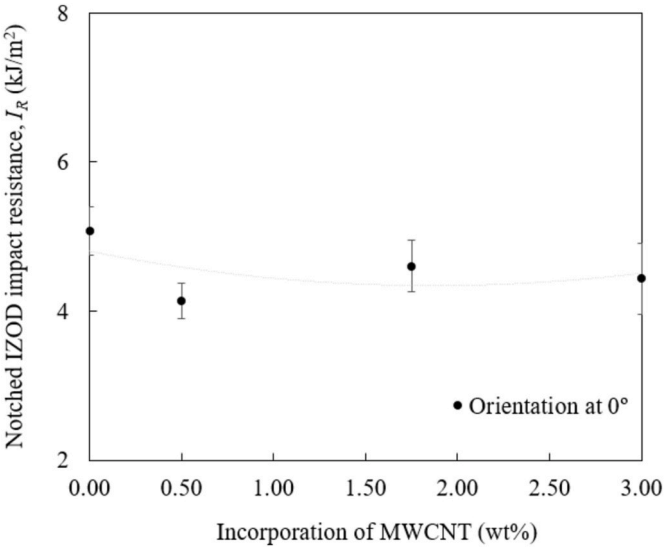

Fig. 15. Notched Izod impact resistance of test specimens produced by SLS as a function of the incorporation of MWCNT.

Table 3
Electrical characterization of PA12-MWCNT composites processed by SLS (surface measurements).

	Surface resistance (Ω)	Surface resistivity (Ω.sqr)	Electrical conductivity (S/cm)
PA12	$4.29 \times 10^{10} \pm 3.83 \times 10^{9}$	$2.29 \times 10^{12} \pm 2.03 \times 10^{11}$	$4.39 \times 10^{-13} \pm 3.75 \times 10^{-14}$
PA12 + 0.50 wt % MWCNT	$1.52 \times 10^{10} \pm 1.24 \times 10^{10}$	$8.11 \times 10^{11} \pm 6.62 \times 10^{11}$	$2.19 \times 10^{-12} \pm 1.98 \times 10^{-12}$
PA12 + 1.75 wt % MWCNT	$4.45 \times 10^{4} \pm 1.02 \times 10^{4}$	$2.37 \times 10^{6} \pm 5.41 \times 10^{5}$	$4.36 \times 10^{-7} \pm 1.00 \times 10^{-7}$
PA12 + 3.00 wt % MWCNT	$2.92 \times 10^{3} \pm 2.63 \times 10^{2}$	$1.56 \times 10^{5} \pm 1.42 \times 10^{4}$	$6.42 \times 10^{-6} \pm 5.87 \times 10^{-7}$

Table 4
Electrical characterization of PA12-MWCNT composites processed by SLS (volume measurements).

	Volume resistance (Ω)	Volume resistivity (Ω.cm)	Electrical conductivity (S/cm)
PA12	$3.16 \times 10^{9} \pm 2.68 \times 10^{8}$	$4.82 \times 10^{11} \pm 4.08 \times 10^{10}$	$2.08 \times 10^{-12} \pm 1.83 \times 10^{-13}$
PA12 + 0.50 wt % MWCNT	$4.08 \times 10^{9} \pm 1.15 \times 10^{9}$	$6.24 \times 10^{11} \pm 1.76 \times 10^{11}$	$1.71 \times 10^{-12} \pm 5.56 \times 10^{-13}$
PA12 + 1.75 wt % MWCNT	$4.29 \times 10^{4} \pm 8.83 \times 10^{3}$	$6.54 \times 10^{6} \pm 1.35 \times 10^{6}$	$1.57 \times 10^{-7} \pm 3.15 \times 10^{-8}$
PA12 + 3.00 wt % MWCNT	$2.93 \times 10^{3} \pm 2.31 \times 10^{2}$	$4.47 \times 10^{5} \pm 3.56 \times 10^{4}$	$2.25 \times 10^{-6} \pm 1.80 \times 10^{-7}$

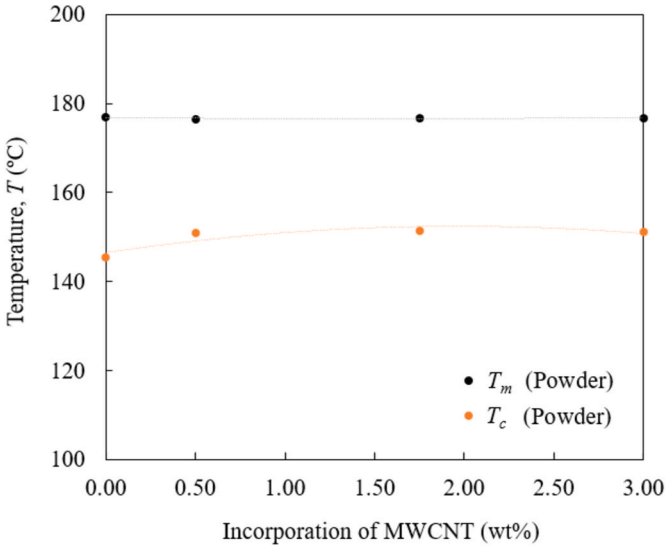

Fig. 16. Melting and crystallization temperatures of SLS powders as a function of the incorporation of MWCNT.

materials demonstrated high thermal stability, without significant mass changes. With TGA analysis, the remaining combustible material at the end of heating was also determined and compared with the theoretical reinforcement content using a random portion of test specimen (Fig. 17 (right)). By subtracting the neat-PA12 residue at 700 °C, it was possible to detect that for the weight percentages of 0.50 wt% and 1.75 wt% of MWCNT, the real reinforcement content was slightly higher than the theoretical, while for 3.00 wt% of MWCNT was slightly lower. These non-significant differences demonstrate the presence of carbon-based

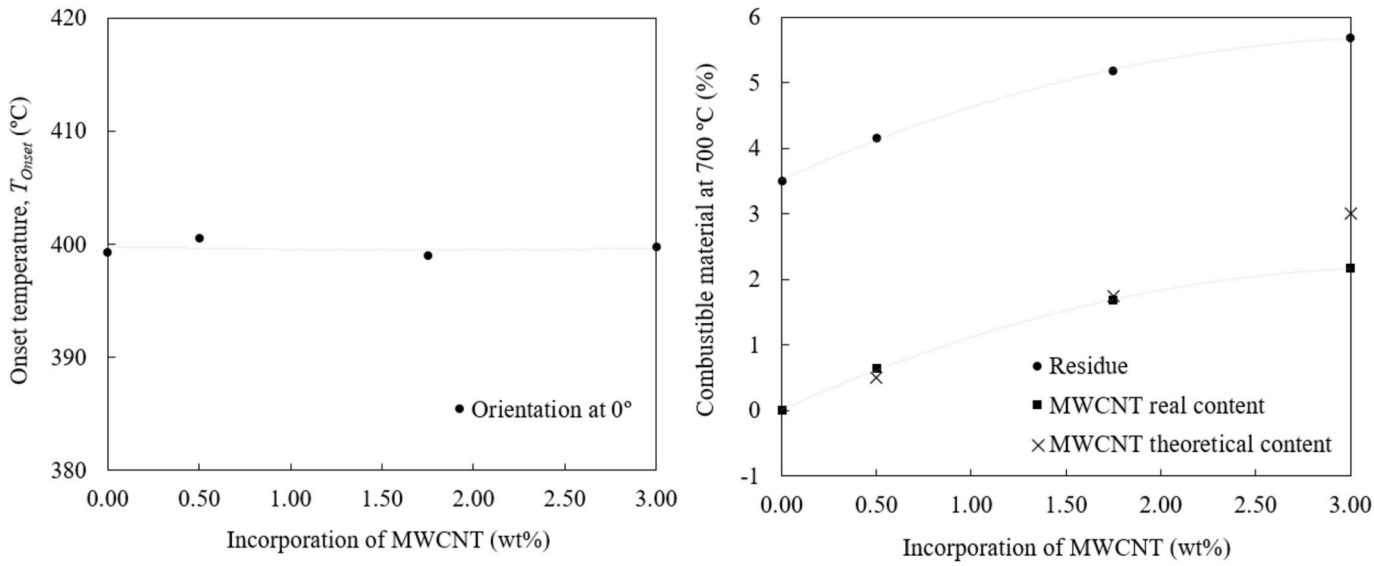

Fig. 17. Onset temperature (left) and combustible material at 700 °C (right) of SLS powders as a function of the incorporation of MWCNT.

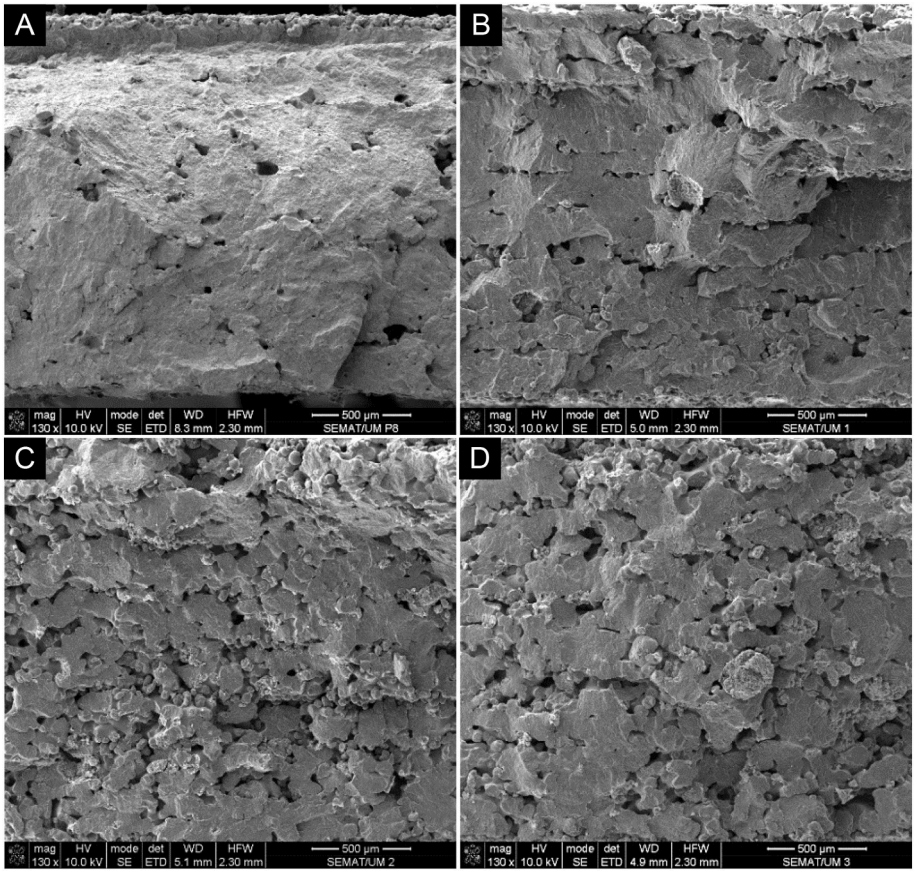

Fig. 18. Cross-section of test specimens produced by SLS with A) PA12, B) PA12 + 0.50 wt% MWCNT, C) PA12 + 1.75 wt% MWCNT and D) PA12 + 3.00 wt % MWCNT.

particles throughout the volume of the test specimens in the planned portions, demonstrating the reliability of the mechanical and electrical characterization previously discussed.

3.7. Morphological characterization

Fig. 18 shows SEM micrographs of the cross-section of test specimens produced by SLS with neat-PA12 and PA12 with 0.50 wt%, 1.75 wt% and 3.00 wt% of MWCNT.

In a first observation at high magnification, the SEM micrographs revealed that the content of porosity of the cross-section increases with the amount of MWCNT, using same conditions of processing. This is a result of a weak interparticle adhesion established between the reinforcement and polymeric matrix. At lower magnification, it is possible to

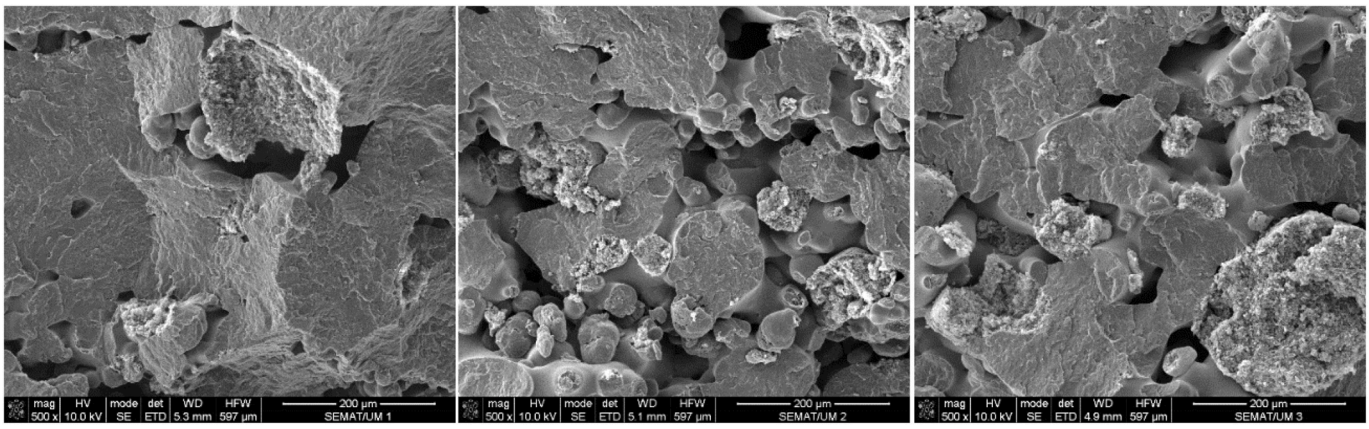

Fig. 19. Cross-section of test specimens produced by SLS with PA12 + 0.50 wt% MWCNT (left), PA12 + 1.75 wt% MWCNT (middle) and PA12 + 3.00 wt% MWCNT (right).

in detail observe agglomerates of MWCNT that were not well dispersed through the process of mechanical mixing (Fig. 19). However, it is also possible to verify that these agglomerates are distributed all over the cross-section of the test specimens, which may explain the reduction in the electrical surface resistance through the conductive path established between the particles of reinforcement, despite the decrease in mechanical properties. With this micro-scale analysis, it was demonstrated that the microstructure developed in the materials during the laser-sintering process is one of the most critical factors influencing the macro-scale properties of neat and/or composite parts produced by SLS, as noticed in previous researches. For instance, a research conducted by Zhou *et al.* [37] revealed that the creation of a porous structure during the processing was responsible for reductions above 80% in the elastic modulus, tensile strength and elongation at break in relation to the polymeric matrix, even incorporating surfactants to improve the dispersion of MWCNT. This highlights the importance of a critical control of the preparation methods and conditions of sintering aiming to minimize the content of porosity of the parts produced in order to obtain a great compromise between mechanical and electrical properties, regardless of the experimental setup.

4. Conclusions and future work

The performance of mechanically-mixed composite materials processed by SLS with PA12 incorporating 0.50 wt%, 1.75 wt% and 3.00 wt % of MWCNT was evaluated in this research. The experiments demonstrated that the processing of these materials requires modifications in the laser-sintering machine (*e.g.* coupling of vibrating powder dispensers, adjustment of fluidisation flow rate) and process parameters (*e.g.* energy density). The thermal analysis indicated that the processing window of the carbon-based composite materials was 6 °C lower than that of conventional PA12. The micro-scale characterization revealed weak interparticle adhesion, agglomerates of MWCNT and porosity, with more pronounced effects for higher weight percentages of reinforcement. In consequence of the resulting microstructure, the tensile and compressive properties of parts produced with composite materials decreased with the increase amount of MWCNT, while the Izod-impact resistance was not significantly modified. In turn, the electrical conductivity increased until 10^{-6} S/cm and the surface resistance decreased until the ESD range, accomplishing the technical requirements of Bosch Car Multimedia S.A. This demonstrated the potential of such carbon-based materials for the production of cost-effective components that are in direct contact with ESD sensitive devices, such as pick-and-place systems used for the positioning of printed circuit boards, where ESD protection is mandatory and mechanical efforts are not critical. The valuable capability of SLS to achieve promising results with low percolation thresholds enabled by the absence of compacting sources, combined with its potential to produce several parts per batch with high geometric flexibility, makes this a promising technology for the production of parts for a variety of other industrial applications. In future work, smaller intervals of weight percentages of incorporation between 0.50 wt% and 1.75 wt% of MWCNT will be considered aiming to obtain a valuable compromise between mechanical and electrical properties within the ESD range. Besides the value of energy density, the laser-sintering process will be optimized with regard to other operating parameters for the most promising materials in order to ensure a quality printability and maximum outputs. The size and shape of the powder particles before and after the preparation methods should be analysed as well. Pre-treatments and/or complementary mixing methods may also be considered in future work in an attempt to improve the adhesion of MWCNT with the matrix, enhancing its dispersion and distribution throughout the cross-section of the parts with the minimum possible cost.

CRediT author statement

A.C. Lopes: Conceptualization, Methodology, Formal analysis, Investigation, Writing - Original Draft. **A.M. Sampaio:** Formal analysis, Validation, Writing - Review & Editing, Supervision, Project administration, Funding acquisition. **A.J. Pontes:** Formal analysis, Validation, Writing - Review & Editing, Supervision, Project administration, Funding acquisition.

Data availability

The raw/processed data required to reproduce these findings cannot be shared at this time as the data also forms part of an ongoing study.

Declaration of competing interest

The authors declare that they have no known competing financial interests or personal relationships that could have appeared to influence the work reported in this paper.

Acknowledgements

This work was co-funded by the European Regional Development Fund through the Operational Competitiveness and Internationalization Programme (COMPETE 2020) [Project No. 47108, “SIFA”; Funding Reference: POCI-01-0247-FEDER-047108] and by the Foundation for Science and Technology (FCT) through the PhD scholarship 2020.04520.BD.

References

[1] A.C. Lopes, A.M. Sampaio, C.S. Silva, A.J. Pontes, Prediction of SLS parts properties using reprocessing powder, Rapid Prototyp. J. 27 (2021) 496–506, https://doi.org/10.1108/RPJ-04-2020-0076.

[2] R.D. Goodridge, C.J. Tuck, R.J.M. Hague, Laser sintering of polyamides and other polymers, Prog. Mater. Sci. 57 (2012) 229–267, https://doi.org/10.1016/j.pmatsci.2011.04.001.

[3] J. Kruth, G. Levy, R. Schindel, T. Craeghs, E. Yasa, Consolidation of polymer powders by selective laser sintering, Proc. 3rd Int. Conf. Polym. Mould. Innov. (2008) 15–30.

[4] D.L. Bourell, T.J. Watt, D.K. Leigh, B. Fulcher, Performance limitations in polymer laser sintering, Phys. Procedia 56 (2014) 147–156, https://doi.org/10.1016/j.phpro.2014.08.157.

[5] S. Dadbakhsh, L. Verbelen, O. Verkinderen, D. Strobbe, P. Van Puyvelde, J. P. Kruth, Effect of PA12 powder reuse on coalescence behaviour and microstructure of SLS parts, Eur. Polym. J. 92 (2017) 250–262, https://doi.org/10.1016/j.eurpolymj.2017.05.014.

[6] D. Drummer, D. Rietzel, F. Kühnlein, Development of a characterization approach for the sintering behavior of new thermoplastics for selective laser sintering, Phys. Procedia 5 (2010) 533–542, https://doi.org/10.1016/j.phpro.2010.08.081.

[7] M. Schmid, A. Amado, K. Wegener, Materials perspective of polymers for additive manufacturing with selective laser sintering, J. Mater. Res. 29 (2014) 1824–1832, https://doi.org/10.1557/jmr.2014.138.

[8] S. Yuan, F. Shen, C.K. Chua, K. Zhou, Polymeric composites for powder-based additive manufacturing: materials and applications, Prog. Polym. Sci. 91 (2019) 141–168, https://doi.org/10.1016/j.progpolymsci.2018.11.001.

[9] M. Picard, A.K. Mohanty, M. Misra, Recent advances in additive manufacturing of engineering thermoplastics: challenges and opportunities, RSC Adv. 10 (2020) 36058–36089, https://doi.org/10.1039/d0ra04857g.

[10] F. Qi, N. Chen, Q. Wang, Preparation of PA11/BaTiO3 nanocomposite powders with improved processability, dielectric and piezoelectric properties for use in selective laser sintering, Mater. Des. 131 (2017) 135–143, https://doi.org/10.1016/j.matdes.2017.06.012.

[11] S. Eshraghi, M. Karevan, K. Kalaitzidou, S. Das, Processing and properties of electrically conductive nanocomposites based on polyamide-12 filled with exfoliated graphite nanoplatelets prepared by selective laser sintering, Int. J. Precis. Eng. Manuf. 14 (2013) 1947–1951, https://doi.org/10.1007/s12541-013-0264-y.

[12] F. Qi, N. Chen, Q. Wang, Dielectric and piezoelectric properties in selective laser sintered polyamide 11/BaTiO3/CNT ternary nanocomposites, Mater. Des. 143 (2018) 72–80, https://doi.org/10.1016/j.matdes.2018.01.050.

[13] A. Asadi, K. Kalaitzidou, Process-structure-property relationship in polymer nanocomposites, in: F. Marotti de Sciarra, P. Russo (Eds.), Exp. Charact. Predict. Mech. Therm. Model. Nanostructures Their Polym, Compos., 2018, pp. 25–100, https://doi.org/10.1016/B978-0-323-48061-1.00002-6.

[14] C.A. Chatham, T.E. Long, C.B. Williams, A review of the process physics and material screening methods for polymer powder bed fusion additive manufacturing, Prog. Polym. Sci. 93 (2019) 68–95, https://doi.org/10.1016/j.progpolymsci.2019.03.003.

[15] V. Francis, P.K. Jain, Advances in nanocomposite materials for additive manufacturing, Int. J. Rapid Manuf. 5 (2015) 215–233, https://doi.org/10.1504/IJRAPIDM.2015.074804.

[16] P. Parandoush, D. Lin, A review on additive manufacturing of polymer-fiber composites, Compos. Struct. 182 (2017) 36–53, https://doi.org/10.1016/j.compstruct.2017.08.088.

[17] W. Jing, C. Hui, W. Qiong, L. Hongbo, L. Zhanjun, Surface modification of carbon fibers and the selective laser sintering of modified carbon fiber/nylon 12 composite powder, Mater. Des. 116 (2017) 253–260, https://doi.org/10.1016/j.matdes.2016.12.037.

[18] H. Wu, W.P. Fahy, S. Kim, H. Kim, N. Zhao, L. Pilato, A. Kafi, S. Bateman, J.H. Koo, Recent developments in polymers/polymer nanocomposites for additive manufacturing, Prog. Mater. Sci. 111 (2020), https://doi.org/10.1016/j.pmatsci.2020.100638.

[19] G.V. Salmoria, R.A. Paggi, V.E. Beal, Graded composites of polyamide/carbon nanotubes prepared by laser sintering, Lasers Manuf. Mater. Process. 4 (2017) 36–44, https://doi.org/10.1007/s40516-017-0035-1.

[20] A. Nazir, H. Yu, L. Wang, S. Fahad, K. ur R. Naveed, A. Khan, B.U. Amin, T. Lin, M. Usman, T. Elshaarani, F. Haq, Electrical conductivity and electromagnetic interference shielding properties of polymer/carbon composites, J. Mater. Sci. Mater. Electron. 30 (2019) 16636–16650, https://doi.org/10.1007/s10854-019-02043-z.

[21] G.V. Salmoria, R.A. Paggi, A. Lago, V.E. Beal, Microstructural and mechanical characterization of PA12/MWCNTs nanocomposite manufactured by selective laser sintering, Polym. Test. 30 (2011) 611–615, https://doi.org/10.1016/j.polymertesting.2011.04.007.

[22] J. Bai, R.D. Goodridge, R.J.M. Hague, M. Song, Improving the mechanical properties of laser-sintered polyamide 12 through incorporation of carbon nanotubes, Polym. Eng. Sci. 53 (2013) 1937–1946, https://doi.org/10.1002/pen.

[23] J. Bai, R.D. Goodridge, R.J.M. Hague, M. Song, M. Okamoto, Influence of carbon nanotubes on the rheology and dynamic mechanical properties of polyamide-12 for laser sintering, Polym. Test. 36 (2014) 95–100, https://doi.org/10.1016/j.polymertesting.2014.03.012.

[24] J. Bai, R.D. Goodridge, S. Yuan, K. Zhou, C.K. Chua, J. Wei, Thermal influence of CNT on the polyamide 12 nanocomposite for selective laser sintering, Molecules 20 (2015) 19041–19050, https://doi.org/10.3390/molecules201019041.

[25] R.A. Paggi, V.E. Beal, G.V. Salmoria, Process optimization for PA12/MWCNT nanocomposite manufacturing by selective laser sintering, Int. J. Adv. Manuf. Technol. 66 (2013), https://doi.org/10.1007/s00170-012-4474-8, 1977–1985.

[26] S. Yuan, J. Bai, C.K. Chua, J. Wei, K. Zhou, Material evaluation and process optimization of CNT-coated polymer powders for selective laser sintering, Polymers 8 (2016), https://doi.org/10.3390/polym8100370.

[27] S. Yuan, Y. Zheng, C.K. Chua, Q. Yan, K. Zhou, Electrical and thermal conductivities of MWCNT/polymer composites fabricated by selective laser sintering, Compos. Part A Appl. Sci. Manuf. 105 (2018) 203–213, https://doi.org/10.1016/j.compositesa.2017.11.007.

[28] L.J. Tan, W. Zhu, K. Zhou, Recent progress on polymer materials for additive manufacturing, Adv. Funct. Mater. 30 (2020), https://doi.org/10.1002/adfm.202003062.

[29] EOS GmbH, PA2200 Balance 1.0 Technical Data Sheet, 2018. www.eos.info.

[30] NANOCYL, NC7000 Technical Data Sheet V08, 2016. www.nanocyl.com.

[31] ASTM, ASTM D695 - Standard Test Method for Compressive Properties of Rigid Plastics, 2002.

[32] ISO, ISO 527 Plastics — Determination of Tensile Properties, 1996.

[33] ASTM, ASTM D256 - Standard Test Methods for Determining the Izod Pendulum Impact Resistance of Plastics, 2004.

[34] ISO, ISO 11357 Plastics — Differential Scanning Calorimetry, DSC), 2016.

[35] ASTM, ASTM E1131 08 - Standard Test Method for Compositional Analysis by Thermogravimetry, 2008, https://doi.org/10.1520/E1131-08.2.

[36] M. Launhardt, A. Wörz, A. Loderer, T. Laumer, D. Drummer, T. Hausotte, M. Schmidt, Detecting surface roughness on SLS parts with various measuring techniques, Polym. Test. 53 (2016) 217–226, https://doi.org/10.1016/j.polymertesting.2016.05.022.

[37] M. Zhou, W. Zhu, S. Yu, Y. Tian, , Selective laser sintering of carbon nanotube–coated thermoplastic polyurethane: mechanical, electrical, and piezoresistive properties, Compos. Part C Open Access 7 (2022), 100212, https://doi.org/10.1016/j.jcomc.2021.100212.